Journal of Applied Polymer Science

Thermally exfoliated graphene oxide reinforced fluorinated pentablock poly(L-lactide-*co*-ε-caprolactone) electrospun scaffolds: Insight into antimicrobial activity and biodegradation

Burcu Saner Okan,[1] Azucena Marset,[1] Jamal Seyyed Monfared Zanjani,[2] Pınar Akkus Sut,[3] Ozlem Sen,[3] Mustafa Çulha,[3] Yusuf Menceloglu[2]

[1]Sabanci University Nanotechnology Research and Application Center, Tuzla Istanbul 34956, Turkey

[2]Faculty of Engineering and Natural Sciences, Advanced Composites and Polymer Processing Laboratory, Sabanci University, Tuzla Istanbul 34956, Turkey

[3]Department of Genetics and Bioengineering, Faculty of Engineering, Yeditepe University, Atasehir, Istanbul 34755, Turkey

Correspondence to: B. S. Okan (E-mail: bsanerokan@sabanciuniv.edu)

ABSTRACT: Three-dimensional fluorinated pentablock poly(L-lactide-*co*-ε-caprolactone)-based scaffolds were successfully produced by the incorporation of thermally exfoliated graphene oxide (TEGO) as an antimicrobial agent with an electrospinning technique. In a ring-opening polymerization, the fluorinated groups in the middle of polymer backbone were attached with a perfluorinated reactive stabilizer having oxygen-carrying ability. The fiber diameter and its morphologies were optimized through changes in TEGO amount, voltage, polymer concentration, and solvent type to obtain an ideal scaffold structure. Instead of the widely used graphene oxide synthesized by Hummer's method, TEGO sheets having a low amount of oxygen produced by thermal expansion were integrated into the fiber structure to investigate the effect of the oxygen functional groups of TEGO sheets on the degradation and antimicrobial activity of the scaffolds. There was no antimicrobial activity in TEGO-reinforced scaffolds in the *in vitro* tests in contrast to the literature. This study confirmed that a low number of oxygen functional groups on the surface of TEGO restricted the antimicrobial activity of the fabricated composite scaffolds. © 2016 Wiley Periodicals, Inc. J. Appl. Polym. Sci. **2016**, *133*, 43490.

KEYWORDS: biodegradable; copolymers; electrospinning; graphene and fullerenes; nanotubes; surfaces and interfaces

Received 20 November 2015; accepted 30 January 2016

DOI: 10.1002/app.43490

INTRODUCTION

Biodegradable scaffolds get a lot of attention in the fields of tissue engineering, wound healing, and organ transplantation for use as templates in tissue regeneration.[1–3] Synthetic biodegradable polymers are used for the production of three-dimensional polymeric scaffolds by electrospinning; this is a widely used and simple technique for fabricating nano and submicrometer fibers. These types of three-dimensional electrospun fiber networks provide high porosity, high surface area, and optimal mechanical strength and favor the attachment, proliferation, and differentiation of various cells; drug loading; and mass transfer properties in tissue engineering applications.[4,5] Among biodegradable polymers, polycaprolactone (PCL) is a widely used synthetic biodegradable polymer that is compatible with a wide range of drugs. However, PCL has some drawbacks, such as its longer degradation period over 14 months and lower hydrophilicity.[6] In addition, polylactide (PLA) is another biocompatible and resorbable polymer; it provides higher mechanical properties, a high porosity, and a much shorter half-life.[7] It is possible to combine the characteristic properties of each biodegradable polymer by the application of blending and copolymerization techniques.[8,9] In one study, PCL/PLA-based copolymer synthesized by gel-pressing procedure was used in cartilage regeneration.[10] In another study, poly(D,L-lactide)/PCL blends were prepared with solution phase for use in liver transplants because of their ability to promote the adhesion, proliferation, and growth of cells.[11] The growing demand for scaffolds having enhanced physical, mechanical, thermal, and biological properties has led to the development of newly designed polymeric materials. At this point, the attachment of fluorinated groups in the polymer structure provides the ability to bind, transport, and unload oxygen in the body. Also, these groups have the advantage of being biologically inert and are easily excreted from the body as a vapor through the lungs.[12,13] Fluorolink,

Additional Supporting Information may be found in the online version of this article

among perfluorinated polyether polymer modifiers, is commercially available and is widely used as a polyol starter in polymer synthesis to improve the oxygen-carrying ability of biodegradable polymers. Saner and Menceloglu[14] synthesized branched pentablock copolymers of PCL and PLA with fluorocarbon surfactants as reactive stabilizers in the medium of supercritical carbon dioxide via a sequential ring-opening polymerization. Fluoroligomers as surface modifiers in polymers provide passive surface properties in medical applications.[15]

To provide multifunctionality, nanomaterials are also integrated into the polymer microstructure during the manufacturing process.[16,17] Graphene is a promising reinforcing agent because of its two-dimensional structure and unique mechanical, electrical, and thermal properties.[18] There have been several studies on the incorporation of graphene-based materials to improve the characteristic properties of electrospun polymeric fibers.[19] For instance, Su *et al.*[20] incorporated 1 wt % multiwalled carbon nanotubes into the microstructure of randomly oriented poly (ethylene oxide) electrospun fibers; this enhanced the tensile strength by approximately 240% and created conducting paths in the hybrid nanomaterials. Song *et al.*[21] synthesized biocomposite nanofiber scaffolds of PCL with different graphene oxide (GO) concentrations with an electrospinning technique in which stems cells adhered, spread, and grew well in these scaffolds. In addition, Ramazani and Karimi[22] investigated the morphological, mechanical, and structural properties of PCL/GO and PCL/reduced GO nanofibers produced by an electrospinning process, and fibers containing reduced GO showed a higher tensile strength and modulus because of the higher number of $-CH_2$ groups in their structure. Hsiao *et al.*[23] prepared reduced GO decorated on polyurethane electrospun fibers by a dip-coating and reduction process with hydriodic acid treatment to obtain higher electrical conductivity. In another study, nanocomposites of poly(lactic acid)/polyurethane having a small amount of GO prepared by solution casting showed good antibacterial activity against Gram-positive *Staphylococcus aureus* and Gram-negative *Escherichia coli*.[24] In the reported studies, graphene and its derivatives showed antimicrobial activity and antiviral properties because of the presence of surface-oxygen functional groups that could extract phospholipid membranes of the bacteria and inhibit their growth.[25,26] Therefore, the synthesis technique of GO and the amount of oxygen functional groups carry significant importance in obtaining antimicrobial activity against bacterial and fungal pathogens. GO is mostly obtained from graphite flakes by the application of the Brodie,[27] Staudenmaier,[28] or Hummers and Offeman[29] oxidation methods and then functionalized with several reducing agents, such as hydrazine,[30] hydroquinone,[31] or sodium borohydride[32] to provide better dispersion in polar and nonpolar solvents. In a thermal treatment, graphite oxide is exposed to heat treatment through changes in the temperature from 550 up to 1050 °C, at which the epoxy and hydroxyl groups of GO start to decompose, and evolved gases cause efficient pressure to break down van der Waals forces, which keep the graphene layers together.[33,34] During thermal exfoliation, most functional groups are removed from the surface of GO, and its surface becomes more hydrophobic when compared to that of the commonly used GO. For instance, oxygen content in GO synthesized by Hummer's method is about 30 atom %, whereas thermally exfoliated graphene oxide (TEGO) has 6 atom % oxygen.[35]

In this study, TEGO was integrated into PCL and a PCL-based fluorinated pentablock copolymer during electrospinning to compare the degradation and antimicrobial properties of the produced scaffolds. Among graphene materials, TEGO was chosen to investigate the effect of the surface-oxygen groups on the antimicrobial activity due to its low oxygen content. To the best of our knowledge, there have been several studies on the utilization of GO having high oxygen amount that prepared by Hummer's method and provided antimicrobial activity in the target materials. On the other hand, in this study, we focused on the importance of the GO type and oxygen amount on the antimicrobial properties. The fiber diameter and its morphologies were optimized through changes in the TEGO amount, applied voltage, polymer concentration, and solvent vapor pressure. The structural properties of PCL polymer were tailored by the addition of Fluorolink-D (FLKD), which was used as a perfluorinated reactive stabilizer, and PLA chains. The synthesis of the fluorinated pentablock copolymer with side chains of PCL and PLA was performed via sequential ring-opening polymerization. Herein, FLKD was preferred because of its oxygen-carrying ability, and PLA was used because of its relative ease of processing into the fiber structure. The characteristic properties of the commercial PCL polymer were compared to those of newly designed fluorinated pentablock copolymers by structural and spectroscopic analysis techniques. The antimicrobial activity and hydrolytic degradation of the produced scaffolds were carried out under *in vitro* conditions.

EXPERIMENTAL

Materials

The following materials were used for polymer synthesis and the electrospinning process: ε-caprolactone monomer (99%, Aldrich), PCL pellets [weight-average molecular weight (M_w) = 80k Da, Aldrich], L-lactide monomer (98%, Aldrich), tin(II) ethyl hexanoate [$Sn(Oct)_2$; 97%, Sigma], methanol (CH_3OH; 99.7%, Sigma-Aldrich), dichloromethane (99.5%, Sigma-Aldrich), *N,N*-dimethyl formamide (DMF; 99%, Sigma-Aldrich), and acetone (99.5%, Sigma-Aldrich). FLKD (M_w = 2000 g/mol) was supplied by Solvay Chemicals. TEGO (grade 2) was purchased from Nanografen Co. The materials used for the antimicrobial tests were agar (Sigma-Aldrich), yeast extract (Sigma-Aldrich), peptone from casein pancreatic digest (Sigma-Aldrich), and sodium chloride (Sigma-Aldrich; 99%).

Fluorinated Pentablock Copolymer Synthesis

Fluorinated pentablock copolymer (PCL–PLA–FLKD–PLA–PCL) was synthesized by bulk polymerization in two steps: fluorinated prepolymer synthesis and block copolymer synthesis; these were explained in detail in our previous publication.[14] In the first step, the fluorinated prepolymer was synthesized by ring-opening polymerization of L-lactide in the presence of FLKD as a perfluorinated linear diol and $Sn(Oct)_2$ as a catalyst at 130 °C for 8 h under an inert atmosphere. The molar ratio of FLKD to L-Lactide was adjusted to 1:20. At the end of the

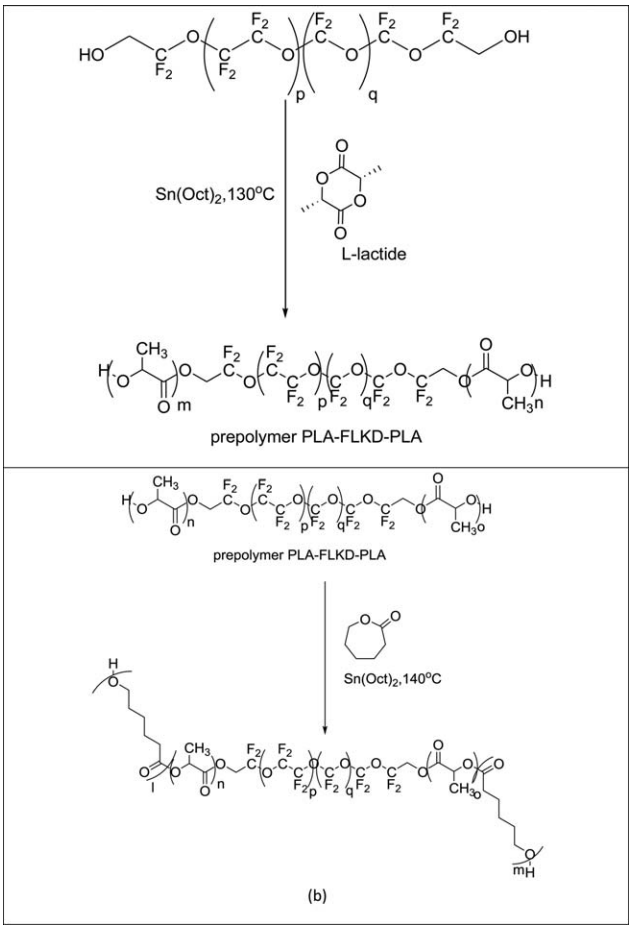

Figure 1. (a) Reaction scheme of fluorinated triblock prepolymer PLA–FLKD–PLA and (b) the reaction scheme of fluorinated pentablock copolymer PCL–PLA–FLKD–PLA–PCL.

reaction, the mixture was gradually diluted with CH_2Cl_2 and then poured into an excess of cold CH_3OH, and the polymer product was precipitated, filtered, and dried at room temperature *in vacuo*. The reaction mechanism of fluorinated triblock prepolymer is shown in Figure 1(a). In the second step, the synthesized fluorinated prepolymer was reacted with ε-caprolactone with $Sn(Oct)_2$ as a catalyst at 140 °C for 18 h for chain elongation. Then, the reaction mixture was redissolved in CH_2Cl_2 and poured into cold CH_3OH for recrystallization (0 °C, 48 h). The resulting product was filtered and washed with CH_3OH and dried *in vacuo* for 6 days to evaporate the solvent. The synthesis route of pentablock fluorinated polymer is represented in Figure 1(b). Both prepolymer and pentablock copolymer reactions were conducted in solvent-free media via bulk polymerization.

A detailed characterization of fluorinated triblock prepolymer (PLA–FLKD–PLA) and fluorinated pentablock copolymer (PCL–PLA–FLKD–PLA–PCL) is given in our previous publication.[14]

Scaffold Production by Electrospinning Process

TEGO sheets with weight percentages of 0.05, 0.1, and 0.2 were dispersed in a acetone/DMF mixture (4:1 v/v) with a probe sonicator for 5 min. Then, PCL polymer (12 wt %) and pentablock copolymer PCL–PLA–FLKD–PLA–PCL (40 and 50 wt %) were dissolved in the TEGO suspension solutions and stirred for 48 h at 40 °C to obtain stabilized and homogeneous electrospun solutions. The internal diameter of the nozzle was 0.8 mm. The syringe was connected to a high-voltage regulated direct-current power supply (HV Power Supply, ES30P-10W). A constant volume flow rate was maintained via a syringe-type infusion pump (NE-1000 Programmable Syringe Pump, New Era). We performed electrospinning process with PCL and TEGO/PCL electrospun solutions with a constant nozzle–collector distance of 10 cm by tailoring the applied voltage in the range 10–20 kV and the flow rate between 9 and 20 μL/min. Fluorinated pentablock copolymer and TEGO-reinforced fluorinated pentablock copolymer fibers were produced with a constant flow rate of 9–10 μL/min through changes in the nozzle–collector distance between 10 and 20 cm and the applied voltage in the range of 10–20 kV. All electrospinning processes were performed under ambient conditions (room temperature = 25 °C)

Characterization

Weight average molecular weight (M_w) and number-average molecular weight (M_n) values of the synthesized polymers were determined with Malvern Viscotek-TDAmax gel permeation chromatograph with DMF used as the eluent. The functional groups and structural properties of the polymers and fibers were investigated by Thermo Scientific Nicolet iS10 Fourier transform infrared spectrometer. Renishaw inVia Reflex Raman spectrometer was used to detect the presence of graphene in the fiber structure. X-ray diffraction (XRD) analysis was performed with a Bruker D-8 Advanced diffractometer. Thermal degradation behaviors of the electrospun TEGO-reinforced PCL and fluorinated pentablock copolymer fibers were examined with Netzsch thermogravimetric analyzer. Thermogravimetric analysis curves of these produced fibers with related explanations are given in Figures S1 and S2 (see the Supporting Information), and the decomposition temperatures and final residue of the neat and TEGO-reinforced fibers are shown in Tables S1 and S2 (see the Supporting Information). The surface morphologies of the fibers were analyzed by a Leo Supra 35VP field emission scanning electron microscope. The average diameters of electrospun fibers were calculated with Image J software.

Hydrolytic Degradation

Hydrolytic degradation of neat fibers, TEGO-reinforced PCL fibers, and TEGO-reinforced fluorinated pentablock fibers was carried out in a phosphate-buffered saline (PBS) solution at pH 7.4. These samples were incubated at 37 °C and stirred at 150 rpm. Then, samples were taken out at select degradation times of 3, 7, 10, and 15 days, and a qualitative evaluation of the fiber degradation was analyzed by scanning electron microscopy (SEM).

Antimicrobial Activity

Antimicrobial activity of the produced fibers was studied by a zone of inhibition test. *S. aureus* (Gram positive) and *E. coli* (Gram negative) were grown in disposable Petri dishes in Luria–Bertani media containing 10 g/L peptone, 5 g/L yeast extract, 10 g/L sodium chloride, and 15 g/L agar. Petri dishes were kept in a shaking incubator at 180 rpm and 37 °C for 18 h.

Table I. Average Fiber Diameters of TEGO-Reinforced PCL Electrospun Fibers as a Function of TEGO amount and Applied Voltage

TEGO (wt %)	Voltage (kV)	Average fiber diameter (nm)
0	20	514 ± 54
0.4	10	359 ± 35
0.8	10	390 ± 42
0.8	15	463 ± 77
0.8	20	543 ± 85
1.6	10	434 ± 63

After cultivation, 200 μL of an overnight culture of bacterial cells was spread on Luria–Bertani agar in the Petri dishes, and then, the fibers were placed on the surface of agar and incubated at 37 °C for 18 h. After incubation, zone inhibition formation around the polymers was analyzed.

Cytotoxicity Test

The cytotoxic effects of the produced scaffolds on cells were quantified by WST-1 colorimetric assay. A volume of 1 mL of Dulbecco's modified Eagle's medium (DMEM) was added to the scaffolds and incubated at 37 °C. After 3, 7, 10, and 15-day incubations, DMEM was collected from the scaffolds. BJ fibroblasts were cultured in DMEM consisting of 10% fetal bovine serum and 1% penicillin streptomycin ampicillin. The cells were kept at 37 °C under atmospheric conditions (95% air and 5% CO_2). BJ fibroblasts were seeded in a 96-well plate and incubated for 24 h. After the incubation period, the cells were treated with DMEM, which was collected from the scaffolds and incubated for 24 h. After that, the media was removed from the BJ fibroblasts and washed with PBS. We calculated the cell viability by measuring the absorbance of the formed formazan salts at 450 nm.

RESULTS AND DISCUSSION

Fabrication of TEGO-Reinforced PCL Electrospun Fibers

Effects of TEGO amount and Applied Voltage on the Morphologies of PCL Fibers. TEGO was incorporated in both PCL and fluorinated pentablock copolymer during the electrospinning process to improve the interfacial interactions between the polymer and graphene layers and also to provide mechanical integrity to the scaffold structure. TEGO sheets had a density of 0.022 g/mL and an average graphene layer number of 25 and contained 6% oxygen, as calculated by X-ray photoelectron spectroscopy (according to the manufacturer). TEGO sheets had a wormlike structure (the SEM images of TEGO are given in Figure S3 in the Supporting Information). The sonication process broke down the van der Waals forces between graphene layers in the TEGO structure and initiated the exfoliation process in the chosen electrospun solvent system. In the initial study, the morphologies and fiber diameters of the TEGO-reinforced PCL electrospun fibers were tailored through changes in the TEGO amount and applied voltage. Table I presents the average fiber diameters of the TEGO-reinforced PCL electrospun fibers as a function of TEGO amount and applied voltage. The polymer concentration, flow rate, and nozzle–collector distance were kept constant in each fiber production. After the incorporation of TEGO, the fiber diameter decreased because of the dense stacking of graphene layers in the polymeric structure and electrostatic interactions between the negatively charged graphene sheets and the positively charged PCL polymer. As the TEGO amount increased in the electrospun solutions, the variations occurred in the electrostatic balance between graphene and its carrier polymer, and thus, the fiber diameter increased.

Figure 2 shows SEM images of TEGO-reinforced PCL electrospun fibers produced by changing TEGO amount and keeping other electrospun process parameters constant. Phase separation was observed in some regions of the fibers reinforced by 0.4 and 0.8 wt % TEGO. This stemmed from the instabilities of the liquid jet during electrospinning and the formation of two distinct TEGO-rich and polymer-rich regions in the fiber structure. On the other hand, as the TEGO amount increased, polymer solution reached the saturation point, and continuous fiber network formation was observed. In addition, the fiber diameter increased with increasing amount of TEGO.

The effects of applied voltage on the morphologies and fiber diameters of TEGO-reinforced PCL electrospun fibers were investigated by SEM. Figure 3 shows the SEM images of TEGO-reinforced PCL electrospun fibers obtained at applied voltages of 10, 15, and 20 kV. The fiber diameter gradually increased with increasing applied voltage and a constant amount of TEGO. As the applied voltage increased, a charged jet travelling to the collector became faster, and the solvent had less time to evaporate; thus, the fiber diameter increased.

Structural Characterization of TEGO-Reinforced PCL Fibers. Raman spectroscopy is an effective technique for detecting the presence of graphene in the fiber structure, and it allows one to identify graphene peaks and defects. Figure 4 shows the Raman spectra for PCL fibers, PCL/0.8 wt % TEGO fibers, and TEGO sheets. The Raman spectrum of TEGO had three main peaks at 1338, 1580, and 2750 cm^{-1}, which corresponded to D, G, and 2D peaks, respectively. The PCL fibers had characteristic Raman peaks at 3100–2800 cm^{-1} due to C—H stretching vibrations, 1060–1106 cm^{-1} related to skeletal vibrations, and 1281–1305 cm^{-1} due to methylene groups.[36] Also, the peak at 1726 cm^{-1} was attributed to the C=O bond of PCL. In the Raman spectrum of TEGO-reinforced PCL fibers, G peak of TEGO appeared at 1580 cm^{-1}, the peak belonging to PCL at 1300 cm^{-1} became wider, and D peak of TEGO sheets overlapped with the methylene signals of PCL. Consequently, Raman spectroscopy analysis showed the presence of TEGO sheets in the electrospun fibers.

The changes in the crystallinity of PCL electrospun fibers with increasing TEGO amount were investigated with XRD. XRD patterns of TEGO sheets, PCL, and PCL/TEGO electrospun fibers with different TEGO contents are displayed in Figure 5. TEGO had a characteristic (002) peak at 26.8 °. PCL fibers had (110) and (200) crystalline peaks at 21.3 and 23.8 °, respectively.[37] After the addition of TEGO into the fiber structure, crystalline peaks of PCL shifted slightly toward higher angles, and the peak intensities decreased because of the intercalation of polymer chains through

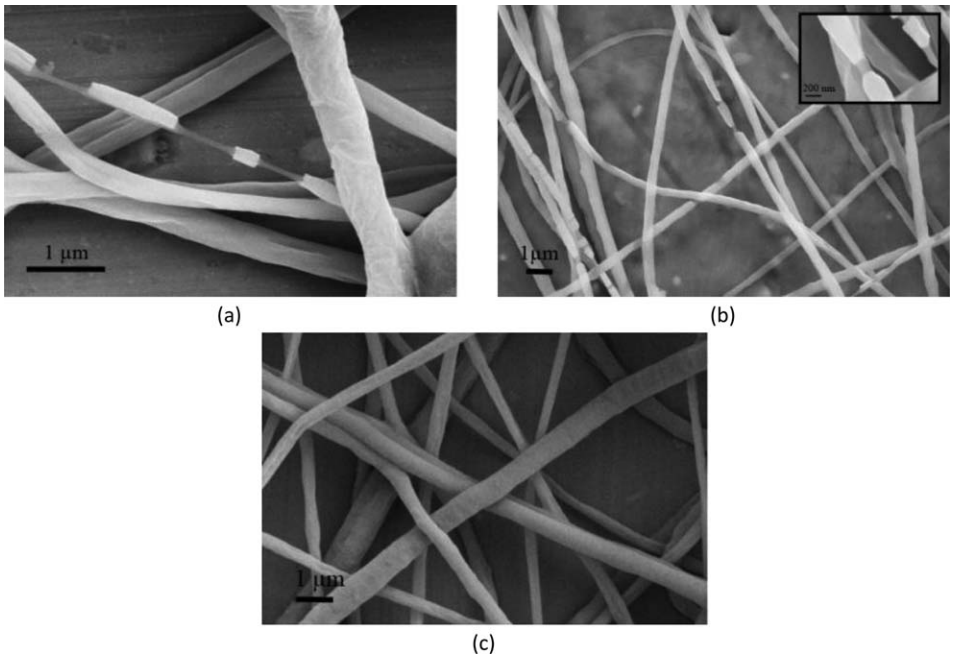

Figure 2. SEM images of (a) PCL/0.4 wt % TEGO, (b) PCL/0.8 wt % TEGO, and (c) PCL/1.6 wt % TEGO electrospun fibers.

graphene layers under an electric field during electrospinning. Table II summarizes the peak intensity and 2θ values of PCL fibers and TEGO-reinforced PCL fibers.

TEGO-Reinforced Fluorinated Electrospun Fibers

Effects of TEGO amount and applied voltage on the Morphologies of Fluorinated Fibers. The M_n and M_w values of the fluorinated pentablock copolymer PCL–PLA–FLKD–PLA–PCL obtained from gel permeation chromatography analysis were 9936 and 22,003 g/mol, respectively. To produce a uniform fiber structure and prevent bead formation in the electrospinning process, polymers having high molecular weight are required to adjust the proper viscosity of electrospun solutions.[38] Therefore, the concentration of fluorinated pentablock copolymer was increased significantly up to 50 wt % to obtain continuous fiber networks, whereas 12 wt % for the PCL

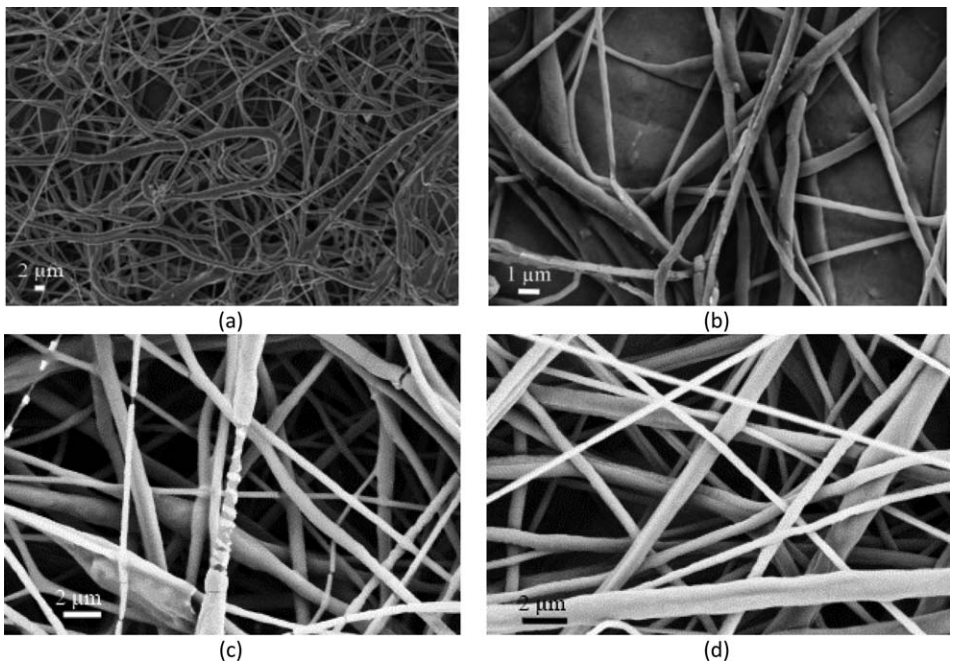

Figure 3. SEM images of (a) neat PCL fibers (flow rate = 20 μm, voltage = 20 kV, nozzle–collector distance = 10 cm) and PCL/0.8 wt % TEGO fibers produced at applied voltages of (b) 10, (c) 15, and (d) 20 kV (flow rate = 9 μL/min, distance = 10 cm).

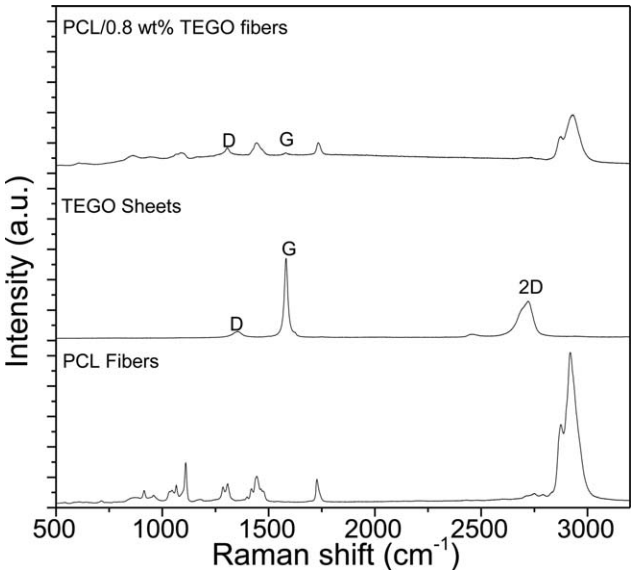

Figure 4. Raman spectra of the TEGO sheets, PCL fibers, and PCL/0.8 wt % TEGO fibers.

polymer was enough to produce electrospun fibers because of its high molecular weight (M_w of PCL = 80,000 g/mol). At this point, the incorporation of TEGO as a nanofiller favored interfacial H bonding between graphene sheets and polymer chains, and this caused an increase in the viscosity of fluorinated polymer solution.[39]

We examined the morphologies of TEGO-reinforced fluorinated pentablock copolymer electrospun fibers by changing the polymer concentration, TEGO amount, and applied voltage. Table III represents the changes in the fiber diameter in terms of different polymer concentrations, applied voltages, and TEGO amount. Figure 6 presents SEM images of 40 wt % fluorinated pentablock copolymer electrospun fibers produced by changing applied voltage and keeping other process parameters constant. As the applied voltage increased, the bead formation was considerably reduced, and fiber diameter increased, as

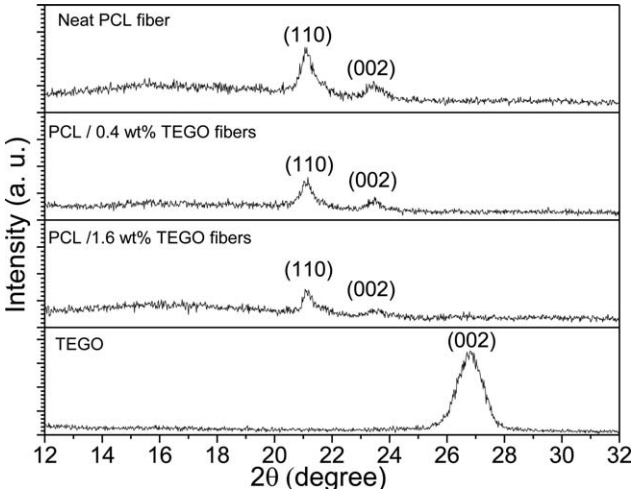

Figure 5. XRD spectra of TEGO sheets, PCL fibers, and TEGO-reinforced PCL electrospun fibers fabricated with different TEGO loadings.

Table II. Peak Intensity and 2θ Values of PCL Fibers and TEGO-Reinforced PCL Fibers

Sample	110 peak (2θ)	Intensity of 110 peak (au)	002 peak (2θ)	Intensity of 002 peak (au)
PCL fibers	21.06	243	23.44	117
PCL/0.4 wt % TEGO fibers	21.16	159	23.48	86
PCL/1.6 wt % TEGO fibers	21.06	142	23.62	70

given in Table III. Herein, higher applied voltage increased the electrostatic repulsion forces between the tip of needle and collector, and this resulted in a higher drawing stress in the jet. These forces decreased the travel time of the polymeric jet between the nozzle and collector, and thus, the formation of beads was considerably reduced, and the fiber diameter was enlarged.[40]

The diameter of fluorinated pentablock copolymer electrospun fibers was tailored through changes in the TEGO amount. To obtain the proper viscosity and reduce the instabilities in the polymer jet, the polymer concentration was increased up to 50 wt %. Also, molecular weight of the polymer indicated the length of polymer chains, and the polymer length defined the amount of entanglement of polymer chains in the solvent. Therefore, polymers having a high molecular weight resulted in increasing chain entanglements in the solution; this was a vital requirement for keeping the continuity of the jet during electrospinning. In this study, polymer concentration in the electrospun solution was kept high and adjusted to 50 wt %. Figure 7 shows SEM images of 50 wt % fluorinated pentablock copolymer electrospun fibers with different TEGO amounts and the neat fibers. Figure 7(a) presents the neat fluorinated pentablock electrospun fibers prepared with a 50 wt % polymer concentration and an average fiber diameter of 150 nm. As shown in Figure 7(b), beads on the fiber string were observed at a 0.2 wt % TEGO loading, and the fiber diameter decreased to 75 nm with the addition of TEGO. Herein, TEGO sheets caused the shrinkage of fibers under an electric field by increasing surface forces during the formation of Taylor cone. On the other hand, as shown in Figure 7(c), as the TEGO content increased, a

Table III. Electrospinning Parameters of Fluorinated Pentablock Copolymer and TEGO-Reinforced Fluorinated Pentablock Copolymer Fibers

Polymer amount (wt %)	TEGO amount (wt %)	Flow rate (μL/min)	Voltage (kV)	Nozzle–collector distance (cm)	Average diameter (nm)
40	0	10	15	10	110 ± 10
40	0	10	20	10	175 ± 18
50	0	9	15	10	150 ± 42
50	0.2	9	15	20	75 ± 30
50	0.4	9	15	20	220 ± 87

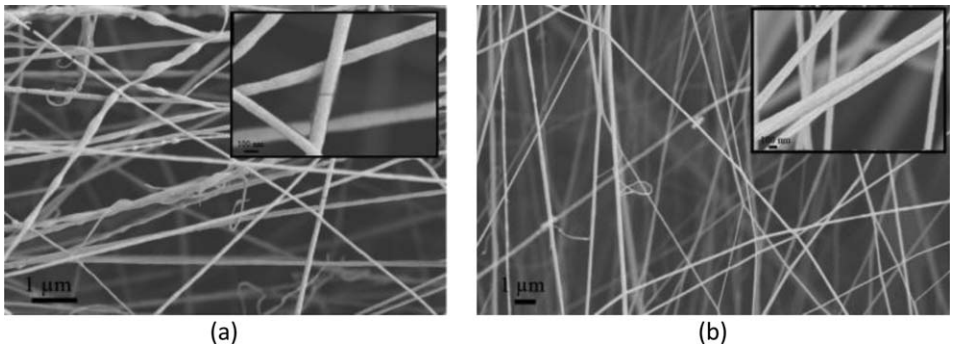

Figure 6. SEM images of 40 wt % fluorinated pentablock copolymer electrospun fibers (solvent = 4:1 v/v acetone/DMF) produced at applied voltages of (a) 15 and (b) 20 kV.

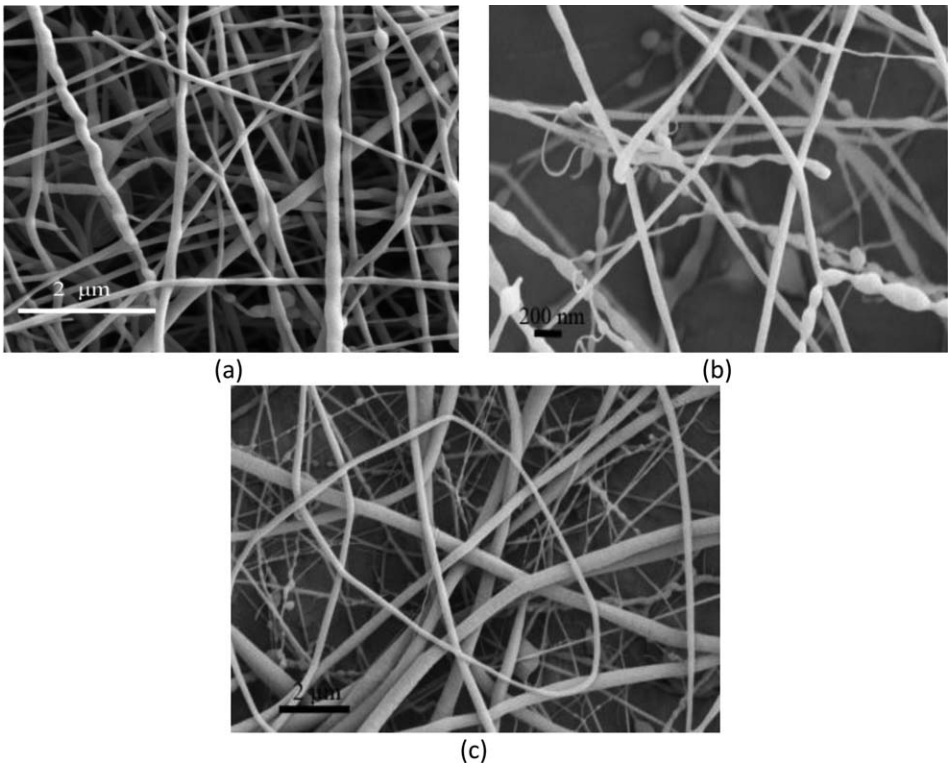

Figure 7. SEM images of (a) 50 wt % fluorinated pentablock copolymer electrospun fibers, (b) 0.2 wt % TEGO/50 wt % fluorinated pentablock copolymer fibers, and (c) 0.4 wt % TEGO/50 wt % fluorinated pentablock copolymer fibers.

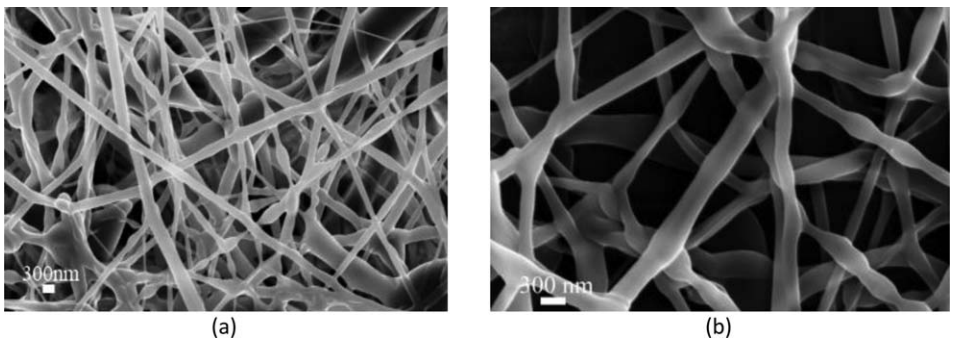

Figure 8. (a,b) SEM images of 50 wt % fluorinated pentablock electrospun fibers at different magnifications (solvent = 1:1 v/v DMF/CH_3OH, applied voltage = 15 kV, and nozzle–collector distance = 10 cm).

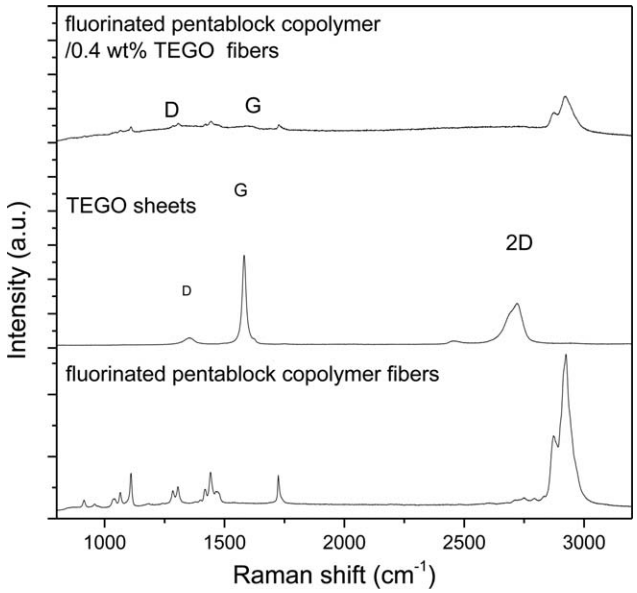

Figure 9. Raman spectra of TEGO sheets, 40 wt % fluorinated pentablock copolymer fibers, and 50 wt % fluorinated pentablock copolymer/0.4 wt % TEGO electrospun fibers.

continuous fiber network without beads was formed, and the fiber diameter increased up to 220 nm because the viscosity of the solution became higher with increasing TEGO amount. In other words, the higher polymer concentration and higher TEGO amount in the electrospun solution enhanced the interactions between the polymer chains and graphene sheets. This led to an increase in the solution viscoelastic behavior.

The type of solvent and its vapor pressure have a significant influence on the diameter and morphology of electrospun fibers.[41] The solvent ratio and polymer concentration were changed in the electrospun solutions to control the diameter of the fluorinated fibers. Herein, the polymer concentration increased up to 50 wt %, and the solvent mixture was changed with DMF and CH_3OH. Herein, the average diameter of these fluorinated fibers increased and became 260 nm; this was compared to fibers with an average diameter of 110 nm produced by the mixture of acetone and CH_3OH. This might have stemmed from the lower affinity between the solvent and polymer, which resulted in an increase in the fiber diameter. Also, the higher polymer concentrations caused an increase in polymer chain entanglements. Figure 8 shows SEM images of 50 wt % fluorinated pentablock electrospun fibers produced with a DMF/CH_3OH mixture (1:1 v/v).

Structural Characterization of TEGO-Reinforced Fluorinated Electrospun Fibers. Figure 9 shows the Raman spectra of TEGO sheets, fluorinated pentablock copolymer fibers, and fluorinated pentablock copolymer/0.4 wt % TEGO fibers. After the addition of TEGO to the electrospun fibers, the D and G peaks at 1340 and 1580 cm^{-1} belonging to TEGO sheets appeared, and the intensity of the characteristic Raman peaks of PCL decreased because the Raman peaks of TEGO overlapped with the polymer peaks and the peaks broadened in these regions. This indicated the presence of TEGO sheets in the structure of the fluorinated electrospun fibers.

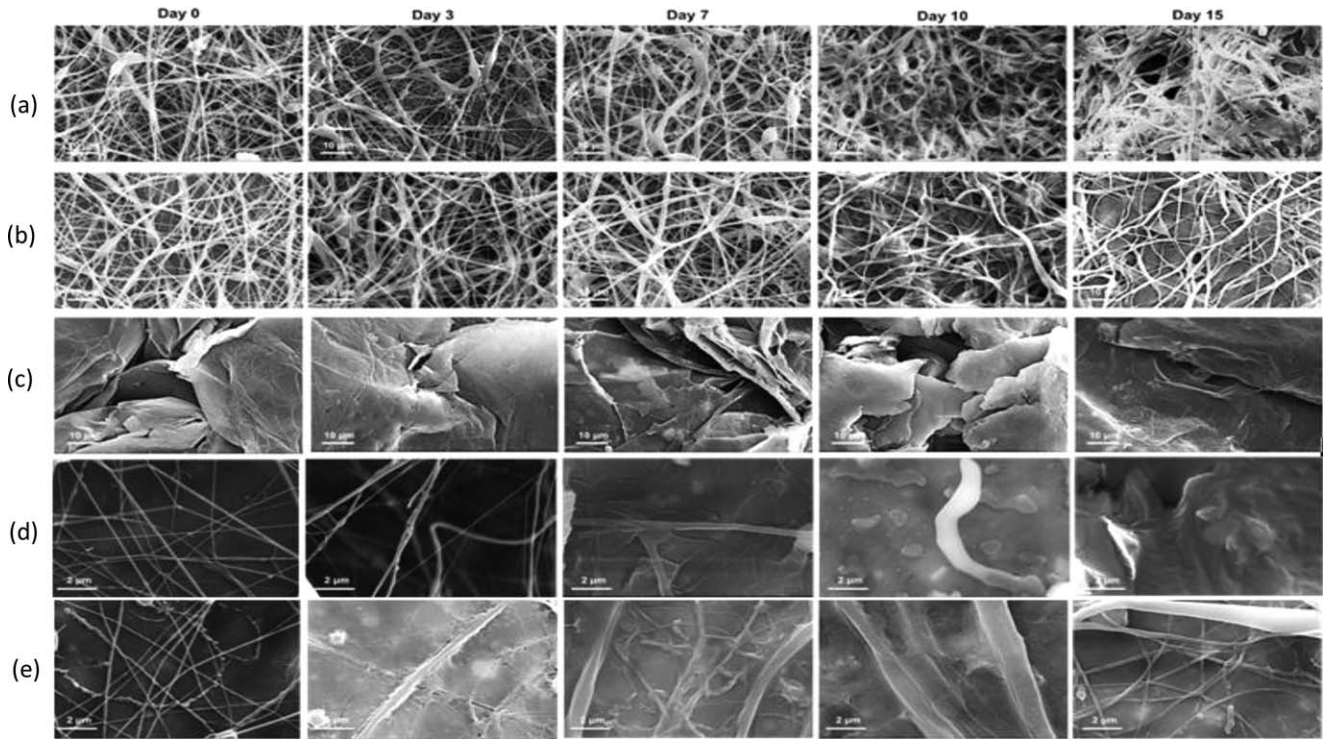

Figure 10. SEM images of the produced scaffolds incubated in PBS for 15 days: (a) 12 wt % PCL fibers, (b) 12 wt % PCL/0.8 wt % TEGO fibers, (c) TEGO sheets, (d) 40 wt % fluorinated pentablock copolymer fibers, and (e) 50 wt % fluorinated pentablock copolymer/0.4 wt % TEGO fibers.

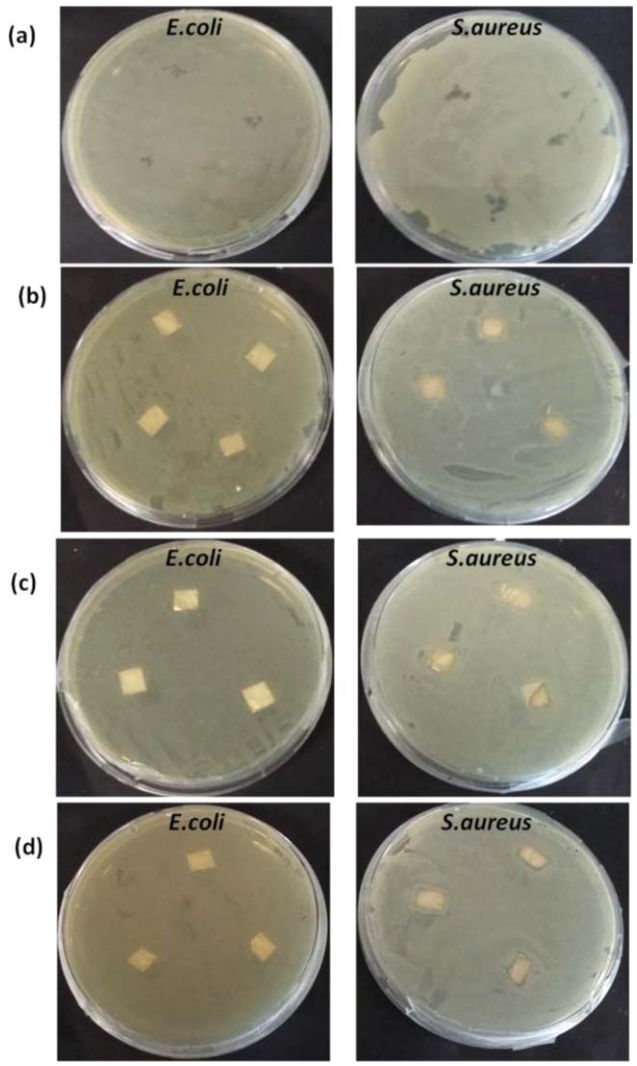

Figure 11. Petri dish images of the antibacterial tests against *S. aureus* and *E. coli*: (a) TEGO sheets, (b) PCL/1.6 wt % TEGO fibers, (c) fluorinated pentablock copolymer/0.2 wt % TEGO fibers, and (d) fluorinated pentablock copolymer/0.4 wt % TEGO fibers. [Color figure can be viewed in the online issue, which is available at wileyonlinelibrary.com.]

Hydrolytic Degradation of TEGO-Reinforced Electrospun Fibers

To study the effect of TEGO on the degradability of the fibers, hydrolytic degradation tests were carried out over electrospun fibers of the neat PCL and fluorinated pentablock copolymers and their TEGO-reinforced electrospun fibers. The morphologies of the samples were investigated over a period of 15 days to observe the degradation behavior of the produced scaffolds. Figure 10 shows the SEM images of TEGO sheets, neat PCL, PCL/TEGO electrospun fibers, neat fluorinated pentablock copolymer fibers, and TEGO-reinforced fluorinated fibers obtained at 3, 7, 10, and 15 days during hydrolytic degradation. In the first 3 days of degradation, no significant changes were observed on the scaffold surface. After 7 days, structural deformation in the scaffolds began, and the fibers became coarse and loose on the 15th day. This indicated the progress of the degradation process. As a result, most of the fibers started to degrade after 15 days. A similar degradation behavior for all fibers indicated that the biodegradability of both PCL and fluorinated pentablock copolymer was not affected by the addition of TEGO sheets. There was also no significant change in the morphologies of TEGO sheets after 15 days of degradation.

Antimicrobial Activity of TEGO-Reinforced Electrospun Fibers

E. coli and *S. aureus* were used as model bacteria to evaluate the antimicrobial activity of TEGO-reinforced electrospun fibers. Neither PCL/TEGO fibers nor fluorinated pentablock copolymer/TEGO fibers exhibited bacterial inactivation because there was no inhibition-zone formation around the materials (Figure 11). In the published literature, however, both neat GO sheets and GO incorporated into polymeric materials inhibited the growth of *E. coli* and *S. aureus* and showed antimicrobial effects.[42,43] In addition, the type of GO used in these published studies was produced by the application of Hummer's method,[29] and this type of GO and its derivatives functionalized by several reducing agents had significant numbers of oxygen groups. This is required to prevent bacterial growth. A higher amount of reactive oxygen species oxidizes fatty acids of bacterial cell membranes and favors the production of lipid peroxides, and thus, a chain reaction leads to the decomposition of the cell membrane and, thus, bacterial cell death.[44,45] However, the type of GO used in this study had a comparably low oxygen content, and its structure contained mostly carbon bonds. Thus, no antimicrobial activity was detected in the performed tests. Consequently, the density of reactive oxygen groups in the structure of antimicrobial agents had a serious effect on the inhibition of bacterial growth.

Cytotoxicity of TEGO-Reinforced Electrospun Fibers

The biocompatibility of TEGO-reinforced electrospun fibers was evaluated with a WST-1 colorimetric assay. The BJ fibroblasts were treated with the media, which were collected from the electrospun fibers on days 3, 7, 10, and 15 of incubation. Figure 12 shows the percentage of cell viability for TEGO-reinforced

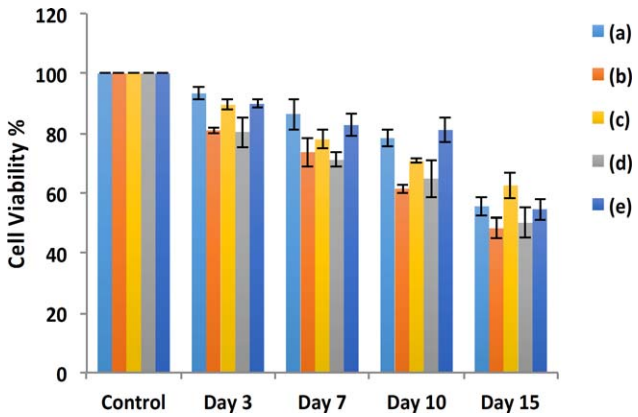

Figure 12. Cell viability of the produced scaffolds incubated in DMEM for 15 days: (a) 12 wt % PCL fibers, (b) 12 wt % PCL/0.8 wt % TEGO fibers, (c) TEGO sheets, (d) 40 wt % fluorinated pentablock copolymer fibers, and (e) 50 wt % fluorinated pentablock copolymer/0.4 wt % TEGO fibers. [Color figure can be viewed in the online issue, which is available at wileyonlinelibrary.com.]

electrospun fibers. In the first 3 days, the cell viability did not significantly decrease in any of the electrospun fibers. After 7 days, the cell viability decreased slightly in the media that were collected from 12 wt % PCL/0.8 wt % TEGO fibers and 40 wt % fluorinated pentablock copolymer fibers when compared to the other electrospun fibers. We found that the media that were collected from 12 wt % PCL fibers and 50 wt % fluorinated pentablock copolymer/0.4 wt % TEGO fibers did not significantly affect the cell viability up to 10 days, whereas the cell viabilities decreased to 61, 70, and 64% for 12 wt % PCL/0.8 wt % TEGO fibers, TEGO sheets, and 40 wt % fluorinated pentablock copolymer fibers, respectively. On the 15th day of the tests, the cell viability of the electrospun fibers, except TEGO sheets (ca. 62%), was calculated to be about 50%. The results show that the addition of 0.4 wt % TEGO to the fluorinated pentablock copolymer fibers increased the cell viability, whereas there was a reduction in the cell viability of 12 wt % PCL/0.8 wt % TEGO fibers.

CONCLUSIONS

In this study, pentablock poly(L-lactide-*co*-ε-caprolactone) with a central fluorinated segment and PLA and PCL side chains was synthesized by sequential ring-opening polymerization, which was conducted in two steps: a fluorinated triblock prepolymer with a central segment of FLKD and PLA side chains and the attachment of PCL side chains to the reactive triblock prepolymer. The fluorinated pentablock copolymer and PCL homopolymer were converted into three-dimensional interconnected porous scaffolds by the integration of TEGO sheets with an electrospinning technique. The fiber diameter and fiber morphologies were tailored through changes in the polymer molecular weight, polymer concentration, applied voltage, type of solvent, and TEGO amount to attain ideal an scaffold structure through the prevention of the formation of beads. The physicochemical properties of TEGO-reinforced scaffolds were examined by SEM, Fourier transform infrared spectroscopy, Raman spectroscopy, and thermogravimetric analysis. The fiber diameter of TEGO-reinforced fluorinated pentablock fibers significantly decreased compared to that of TEGO-reinforced PCL fibers because of the lower molecular weight of the pentablock copolymer. The molecular weight indicated the entanglement of polymer chains in solutions, and this directly affected the solution viscosity. Thus, an ideal scaffold structure with a fluorinated pentablock copolymer was achieved through increases in the polymer concentration up to 50 wt % and the control of the viscosity with the addition of TEGO. In this study, we especially addressed the significant role of surface-oxygen functional groups on the antimicrobial properties of graphene sheets. The type of GO and its synthesis methods directly affected the antimicrobial properties of graphene. TEGO produced by the thermal treatment of GO having a low density of oxygen (6 wt %) in its structure was used as an antimicrobial agent, and TEGO-reinforced scaffolds did not show any antimicrobial activity in *in vitro* studies. Consequently, the amount of surface functional groups in the graphene structure had a significant effect on the inhibition of bacterial growth, and these results brought new insight to the relation between the surface composition of graphene and its antimicrobial properties in biomedical applications.

REFERENCES

1. Marx, V. *Nature* **2015**, *522*, 373.
2. Dvir, T.; Timko, B. P.; Kohane, D. S.; Langer, R. *Nat. Nanotechnol.* **2011**, *6*, 13.
3. Kostruba, A.; Ohar, M.; Kulyk, B.; Zolobko, O.; Stetsyshyn, Y. *Appl. Surf. Sci.* **2013**, *276*, 340.
4. Agarwal, S.; Wendorff, J. H.; Greiner, A. *Polymer* **2008**, *49*, 5603.
5. Sundaramurthi, D.; Krishnan, U. M.; Sethuraman, S. *Polym. Rev.* **2014**, *54*, 348.
6. Hakkarainen, M.; Albertsson, A.-C. *Macromol. Chem. Phys.* **2002**, *203*, 1357.
7. Drumright, R. E.; Gruber, P. R.; Henton, D. E. *Adv. Mater.* **2000**, *12*, 1841.
8. Huang, M.-H.; Li, S.; Vert, M. *Polymer* **2004**, *45*, 8675.
9. Patrício, T.; Bártolo, P. *Proc. Eng.* **2013**, *59*, 292.
10. Jung, Y.; Park, M. S.; Lee, J. W.; Kim, Y. H.; Kim, S.-H.; Kim, S. H. *Biomaterials* **2008**, *29*, 4630.
11. Calandrelli, L.; Calarco, A.; Laurienzo, P.; Malinconico, M.; Petillo, O.; Peluso, G. *Biomacromolecules* **2008**, *9*, 1527.
12. Lowe, K. C. *J. Fluorine Chem.* **2001**, *109*, 59.
13. Riess, J. G. *J. Fluorine Chem.* **2002**, *114*, 119.
14. Saner, B.; Menceloglu, Y. Z.; Bilgin Oncu, N. *High Perform. Polym.* **2007**, *19*, 649.
15. Santerre, P. J. PCT CA2002/000817 **2002**.
16. Su, Z.; Ding, J.; Wei, G. *RSC Adv.* **2014**, *4*, 52598.
17. Kalay, S.; Stetsyshyn, Y.; Lobaz, V.; Harhay, K.; Ohar, H.; Çulha, M. *Nanotechnology* **2016**, *27*, 35703.
18. Geim, A. K. *Science* **2009**, *324*, 1530.
19. Das, S.; Wajid, A. S.; Bhattacharia, S. K.; Wilting, M. D.; Rivero, I. V.; Green, M. J. *J. Appl. Polym. Sci.* **2013**, *128*, 4040.
20. Su, Z.; Li, J.; Li, Q.; Ni, T.; Wei, G. *Carbon* **2012**, *50*, 5605.
21. Song, J.; Gao, H.; Zhu, G.; Cao, X.; Shi, X.; Wang, Y. *Carbon* **2015**, *95*, 1039.
22. Ramazani, S.; Karimi, M. *Mater. Sci. Eng. C* **2015**, *56*, 325.
23. Hsiao, S.-T.; Ma, C.-C. M.; Tien, H.-W.; Liao, W.-H.; Wang, Y.-S.; Li, S.-M.; Chuang, W.-P. *Compos. Sci. Technol.* **2015**, *118*, 171.
24. An, X.; Ma, H.; Liu, B.; Wang, J. *J. Nanomater.* **2013**, *2013*, 1.
25. Krishnamoorthy, K.; Veerapandian, M.; Zhang, L.-H.; Yun, K.; Kim, S. J. *J. Phys. Chem. C* **2012**, *116*, 17280.
26. Pham, V. T. H.; Truong, V. K.; Quinn, M. D. J.; Notley, S. M.; Guo, Y.; Baulin, V. A.; Al Kobaisi, M.; Crawford, R. J.; Ivanova, E. P. *ACS Nano* **2015**, *9*, 8458.
27. Brodie, B. C. *Philos. Trans. R. Soc. London* **1859**, *149*, 249.
28. Staudenmaier, L. *Ber. Dtsch. Chem. Ges.* **1898**, *31*, 1481.
29. Hummers, W. S.; Offeman, R. E. *J. Am. Chem. Soc.* **1958**, *80*, 1339.

30. Stankovich, S.; Dikin, D. A.; Piner, R. D.; Kohlhaas, K. A.; Kleinhammes, A.; Jia, Y.; Wu, Y.; Nguyen, S. T.; Ruoff, R. S. *Carbon* **2007**, *45*, 1558.
31. Wang, G.; Yang, J.; Park, J.; Gou, X.; Wang, B.; Liu, H.; Yao, J. *J. Phys. Chem. C* **2008**, *112*, 8192.
32. Si, Y.; Samulski, E. T. *Nano Lett.* **2008**, *8*, 1679.
33. McAllister, M. J.; Li, J.-L.; Adamson, D. H.; Schniepp, H. C.; Abdala, A. A.; Liu, J.; Herrera-Alonso, M.; Milius, D. L.; Car, R.; Prud'homme, R. K.; Aksay, I. A. *Chem. Mater.* **2007**, *19*, 4396.
34. Saner, B.; Dinç, F.; Yürüm, Y. *Fuel* **2011**, *90*, 2609.
35. Chen, J.; Yao, B.; Li, C.; Shi, G. *Carbon* **2013**, *64*, 225.
36. Sayyar, S.; Murray, E.; Thompson, B. C.; Gambhir, S.; Officer, D. L.; Wallace, G. G. *Carbon* **2013**, *52*, 296.
37. Pant, H. R.; Neupane, M. P.; Pant, B.; Panthi, G.; Oh, H.-J.; Lee, M. H.; Kim, H. Y. *Colloids Surf. B* **2011**, *88*, 587.
38. Bhardwaj, N.; Kundu, S. C. *Biotechnol. Adv.* **2010**, *28*, 325.
39. Tan, Y.; Song, Y.; Zheng, Q. *Nanoscale* **2012**, *4*, 6997.
40. Lee, K. H.; Kim, H. Y.; Bang, H. J.; Jung, Y. H.; Lee, S. G. *Polymer* **2003**, *44*, 4029.
41. Seyyed Monfared Zanjani, J.; Saner Okan, B.; Letofsky-Papst, I.; Yildiz, M.; Menceloglu, Y. Z. *Eur. Polym. J.* **2015**, *62*, 66.
42. Liu, S.; Zeng, T. H.; Hofmann, M.; Burcombe, E.; Wei, J.; Jiang, R.; Kong, J.; Chen, Y. *ACS Nano* **2011**, *5*, 6971.
43. Bora, C.; Bharali, P.; Baglari, S.; Dolui, S. K.; Konwar, B. K. *Compos. Sci. Technol.* **2013**, *87*, 1.
44. Pasquini, L. M.; Sekol, R. C.; Taylor, A. D.; Pfefferle, L. D.; Zimmerman, J. B. *Environ. Sci. Technol.* **2013**, *47*, 8775.
45. Mangadlao, J. D.; Santos, C. M.; Felipe, M. J. L.; de Leon, A. C. C.; Rodrigues, D. F.; Advincula, R. C. *Chem. Commun.* **2015**, *51*, 2886.